Finite Volume Methods for Gradient Flows

Eleanor Byrnes and Payton Howell

June 7, 2024

Abstract

We follow the work of Carillo *et al* [1] in order to gain an understanding of the application of finite volume methods to a non-linear and non-local equation which has a gradient flow structure. Through this process, we investigate their theoretical results and implement their algorithms for a number of problems.

1 Introduction

In Carillo *et al*'s 2014 paper [1], they develop a finite volume scheme to solve the equation

$$\begin{cases} \rho_t & = \nabla \cdot [\rho \nabla (H'(\rho) + V(\mathbf{x}) + W * \rho)], \quad \mathbf{x} \in \mathbb{R}^d, \\ \rho(\mathbf{x}, 0) & = \rho_0(\mathbf{x}) \end{cases}. \tag{1}$$

Here, ρ is some positive probability measure and H, V, and W are different types of energy in the system corresponding to the internal energy, a confinement potential, and an interaction potential respectively. Equation 1 is applicable in a number of contexts (discussed more in Sections 4.2 and 4.3) and is known to have a free energy associated with it given by

$$E(\rho) = \int_{\mathbb{R}^d} H(\rho) + V(\mathbf{x})\rho(\mathbf{x}) d\mathbf{x} + \frac{1}{2} \int_{\mathbb{R}^d} \int_{\mathbb{R}^d} W(\mathbf{x} - y)\rho(\mathbf{x})\rho(\mathbf{y}) d\mathbf{x} d\mathbf{y}. \tag{2}$$

This energy decreases along classical solutions to Equation 1 and yields a gradient flow system in the W_2 norm. We discuss this structure further in Section 2.1. Carillo *et al* utilize this structure to develop a finite volume scheme which is stable, positivity preserving and entropy decreasing. We define and give some intuition to the method in Section 3.1, and replicate some of Carillo *et al*'s proofs in Sections 3.2 and 3.3. We then discuss the implementation of their schemes to various equations of the form of Equation 1 in Section 4.1 and present results in Sections 4.2 and 4.3.

2 Background

2.1 Gradient Flow Structure

As noted in the introduction, our system has a gradient flow structure such that the free energy given in Equation 2 decreases along solutions of Equation 1. As Carillo *et al* [1] note, the time derivative of this quantity is given by

$$\frac{d}{dt} E(\rho) = -\int_{\mathbb{R}^d} \rho |\mathbf{u}|^2 d\mathbf{x} := -I(\rho), \tag{3}$$

where

$$\mathbf{u} = -\nabla \zeta, \text{ and} \tag{4}$$

$$\zeta := \frac{\delta E}{\delta \rho} = H'(\rho) + V(\mathbf{x}) + W * \rho. \tag{5}$$

It's worth noting that, in the context of this class, Equations 3-5 are exactly what we would expect for the form of a gradient flow on W_2 with energy given by Equation 2. Furthermore, this also gives us a form for the continuous energy flux which we can use at each interface. In particular, in one dimension can write this as

$$-\rho\zeta_x = -\rho u = -\rho(H'(\rho) + V(x) + W * \rho)_x. \tag{6}$$

In two or more dimensions, we can use this formula to compute the flux in each direction, replacing the x-derivative with a derivative in the relevant direction.

3 Method

3.1 Method Definition

As Carillo *et al* [1] do, we begin the description of our method by partitioning our domain into cells. Our our probability measure will be represented by the averages of its value over each of these cells. In one dimension our the cells with center x_j will be labelled C_j and if we choose our grid spacing to be uniformly spaced with width Δx our cell averages will be given by

$$\overline{\rho}_j = \frac{1}{\Delta x}\int_{C_j} \rho(\mathbf{x}, t)d\mathbf{x}.$$

Recognize we can write Equation 1 in the form

$$\rho_t = \nabla \cdot \mathcal{F}(\rho, \mathbf{x}).$$

To discretize this equation, we note that so long as our cells are sufficiently small, the right hand side can be approximated by a finite difference of $\mathcal{F}$ over our boundaries. In one dimension this becomes

$$\overline{\rho}_t(x,t) = -\frac{F_{j+\frac{1}{2}}(t) - F_{j-\frac{1}{2}}(t)}{\Delta x}, \tag{7}$$

and in two it becomes

$$\overline{\rho}_t(\mathbf{x},t) = -\left(\frac{F_{i+\frac{1}{2},j}(t) - F_{i-\frac{1}{2},j}(t)}{\Delta x} + \frac{F_{i,j+\frac{1}{2}}(t) - F_{i,j-\frac{1}{2}}(t)}{\Delta y}\right). \tag{8}$$

Here, $F_{j+\frac{1}{2}}$ is the value of our approximation to the flux F given at the right boundary of cell C_j.

We unfortunately have the issue that we don't know the values of our function at our boundaries, only the averages over each cell. Carillo *et al* [1] solve this problem by constructing piecewise linear approximations to the probability measure within each cell. The method first attempts to use a centered finite difference in each cell. If this leads to negative values at the boundaries of a given cell, the slope in that cell is instead selected using a minmod limiter:

$$(\rho_x)_j = \text{minmod}\left(\theta\frac{\overline{\rho}_{j+1} - \overline{\rho}_j}{\Delta x}, \frac{\overline{\rho}_{j+1} - \overline{\rho}_{j-1}}{2\Delta x}, \theta\frac{\overline{\rho}_j - \overline{\rho}_{j-1}}{\Delta x}\right), \tag{9}$$

$$\text{minmod}(z_1, z_2, \dots) = \begin{cases} \min(z_1, z_2, \dots) & z_i > 0 \quad \forall i, \\ \max(z_1, z_2, \dots) & z_i < 0 \quad \forall i, \\ 0 & \text{otherwise.} \end{cases} \tag{10}$$

$\theta = 2$ is used for all examples; this parameter is used to control numerical viscosity by scaling the non centered finite difference schemes for the slope. Using this limiter, we can define the piecewise linear polynomial

$$\tilde{\rho}_j(x) = \overline{\rho}_j + (\rho_x)_j(x - x_j), \quad x \in C_j.$$

Once we have a piecewise linear approximation to ρ we can compute our fluxes and plug them into Equation 7 or 8. To do so, we need to determine approximations of the fluxes given by Equation 6. To approximate the flux u at each boundary, we need to be able to approximate ζ. Discretizing Equation 5 we get that

$$\zeta_j = \Delta x \sum_i W(x_j - x_i)\overline{\rho}_i + H'(\rho_j) + V(x_j). \tag{11}$$

Using these values of ζ we can define the value of u on each boundary through a centered difference,

$$u_{j+\frac{1}{2}} = -\frac{\zeta_{j+1} - \zeta_j}{\Delta x}. \tag{12}$$

We note that the flux across each boundary could move in one of two ways: either it could be flux into the cell on the right from the cell on the left, or flux into the cell on the left from the cell on the right. To determine which of these cases we fall into, we define $u^+_{j+\frac{1}{2}}$ to be the maximum of $u_{j+\frac{1}{2}}$ and 0 and $u^-_{j+\frac{1}{2}}$ to be the minimum of $u_{j+\frac{1}{2}}$ and zero. Notice that at most one of these is non-zero. If $u^+_{j+\frac{1}{2}} \neq 0$, then we have flux leaving the cell C_j and entering the cell C_{j+1} through this boundary, and if $u^-_{j+\frac{1}{2}} \neq 0$ the opposite is true. Effectively, the rate and direction of the flow is controlled by the magnitude of $u_{j+\frac{1}{2}}$ and its sign. Define ρ^E_j and ρ^W_j to be the values of $\tilde{\rho}_j$ on the east and west boundaries of the cell C_j, respectively. Then we may define the approximation to our flux at the right boundary of the jth cell to be

$$F_{j+\frac{1}{2}} = u^+_{j+\frac{1}{2}}\rho^E_j + u^-_{j+\frac{1}{2}}\rho^W_{j+1}. \tag{13}$$

Now that we've determined the right hand sides of 7 and 8 in terms of known quantities, and all that is left is to solve for the time dependence of these ODE systems. If, as Carillo *et al* [1] do, we use a stable and accurate ODE solver such as a third-order strong preserving Runge-Kutta solver we should be able to recover their results. Before we do that, we should briefly discuss the various properties that this scheme has. To do so, we replicate Carillo *et al*'s [1] discussion of these properties in one dimension, and refer the reader to the original paper to see the two-dimensional proofs.

3.2 Positivity Preservation

We now demonstrate the positivity preservation of this method for a first order-Euler discretization of system 7, and leave the demonstration for a higher-order scheme to the reader. Suppose that

$$\Delta t \leq \frac{\Delta x}{2a}, \quad a = \max_j \left\{ u^+_{j+\frac{1}{2}}, -u^-_{j+\frac{1}{2}} \right\}. \tag{14}$$

This is the CFL condition for our system. We also suppose that at some time t the computed solution is positive as desired so that $\overline{\rho}_j \geq 0$ for all j. Then an Euler discretization of Equation 7 yields that

$$\overline{\rho}_j(t + \Delta t) = \overline{\rho}_j(t) - \lambda \left[F_{j+\frac{1}{2}}(t) - F_{j-\frac{1}{2}}(t) \right].$$

Here, $\lambda = \Delta t/\Delta x \leq \frac{1}{2a}$. By the fact that our piece-wise linear approximation to ρ in cell C_j is centered to give $\tilde{\rho}_j(x_j) = \rho_j$, we have that

$$\rho_j = \frac{\rho^W_j + \rho^E_j}{2}.$$

Using Equation 13 and suppressing our dependence on t on the right hand side, we see that:

$$\begin{aligned}
\rho_j(t + \Delta t) &= \frac{1}{2}(\rho^E_j + \rho^W_j) - \lambda \left[u^+_{j+\frac{1}{2}}\rho^E_j + u^-_{j+\frac{1}{2}}\rho^W_{j+1} - u^+_{j-\frac{1}{2}}\rho^E_{j-1} - u^-_{j-\frac{1}{2}}\rho^W_j \right], \\
&= \lambda u^+_{j-\frac{1}{2}}\rho^E_{j-1} + \left(\frac{1}{2} - \lambda u^+_{j+\frac{1}{2}} \right)\rho^E_j + \left(\frac{1}{2} + \lambda u^-_{j-\frac{1}{2}} \right)\rho^W_j - \lambda u^-_{j+\frac{1}{2}}\rho^W_{j+1}.
\end{aligned}$$

This last line is a linear combination of positive things with positive coefficients, thus at our next time step our solution is still positive. Thus the scheme is positivity preserving!

3.3 Entropy Dissipation

To show that solutions to our numerical scheme decrease in free energy (or entropy), as in the original equations, we define a discrete version of the entropy E by

$$E_\Delta(t) = \Delta x \sum_j \left[\frac{1}{2} \Delta x \sum_i W_{j-i} \overline{\rho}_i \overline{\rho}_j + H(\overline{\rho}_j) + V(x_j) \overline{\rho}_j \right]. \tag{15}$$

We also define a discretization of the entropy dissipation functional I by

$$I_\Delta(t) = \Delta x \sum_j (u_{j+\frac{1}{2}})^2 \min_j \left(\rho_j^E, \rho_{j+1}^W \right). \tag{16}$$

If we take a time derivative of Equation 15 we obtain that

$$\begin{aligned} \frac{d}{dt} E_\Delta(t) &= \Delta x \sum_j \left[\Delta x \sum_i W(x_j - x_i) \overline{\rho}_i \frac{d\overline{\rho}_j}{dt} + H'(\overline{\rho}_j) \frac{d\overline{\rho}_j}{dt} + V(x_j) \frac{d\overline{\rho}_j}{dt} \right] \\ &= \Delta x \sum_j \left[\Delta x \sum_i W(x_j - x_i) \overline{\rho}_i + H'(\overline{\rho}_j) + V(x_j) \right] \frac{d\overline{\rho}_j}{dt} \end{aligned}$$

Recall the definition of the discrete velocity field ζ_j given in Equation 11. This is precisely the interior of the brackets. If we recall also the form of our ODE given in Equation 7, this reduces to

$$\frac{d}{dt} E_\Delta(t) = -\Delta x \sum_j \zeta_j \frac{F_{j+\frac{1}{2}} - F_{j-\frac{1}{2}}}{\Delta x} = \sum_j \zeta_j (F_{j+\frac{1}{2}} - F_{j-\frac{1}{2}}).$$

Suppose that we have a pair of sequences $\{f_k\}$ and $\{g_k\}$. A discrete integration by parts relates a pair of sums in a way analogous to a continuous integration by parts, with

$$\sum_{k=m}^{n} f_k (g_{k+1} - g_k) = (f_n g_{n+1} - f_m g_m) - \sum_{k=m}^{n} g_{k+1} (f_{k-1} - f_k).$$

Then a discrete integration by parts, paired with our no-flux boundary condition, reveals that

$$\begin{aligned} \frac{d}{dt} E_\Delta(t) &= -\sum_j (\zeta_j - \zeta_{j+1}) F_{j+\frac{1}{2}}, \\ &= -\Delta x \sum_j u_{j+\frac{1}{2}} F_{j+\frac{1}{2}}, \\ &= -\Delta x \sum_j u_{j+\frac{1}{2}} \left[u^+_{j+\frac{1}{2}} \rho_j^E + u^-_{j+\frac{1}{2}} \rho_{j+1}^W \right]. \end{aligned}$$

Noting that at most one of $u^\pm_{j+\frac{1}{2}}$ is non-zero and the other one is $u_{j+\frac{1}{2}}$,

$$u_{j+\frac{1}{2}} \left[u^+_{j+\frac{1}{2}} \rho_j^E + u^-_{j+\frac{1}{2}} \rho_{j+1}^W \right] \geq u^2_{j+\frac{1}{2}} \min_j (\rho_j^E, \rho_{j+1}^W).$$

Plugging in, we see that

$$\begin{aligned} \frac{d}{dt} E_\Delta(t) &= -\Delta x \sum_j u_{j+\frac{1}{2}} \left[u^+_{j+\frac{1}{2}} \rho_j^E + u^-_{j+\frac{1}{2}} \rho_{j+1}^W \right], \\ &\leq -\Delta x \sum_j (u_{j+\frac{1}{2}})^2 \min_j (\rho_j^E, \rho_{j+1}^W) = -I_\Delta(t). \end{aligned}$$

Thus, our scheme preserves the entropy dissipation property of the original system! Confident in our method, we proceed to its implementation and present some results!

4 Implementation/Results

4.1 Implementation

As mentioned in Section 3.1, in addition to implementing our discretization of the fluxes, we solve our resulting ODE using a three stage third-order strong stability preserving Runge-Kutta solver, SSPRK(3,3), from Gottlieb *et al* [2]. Let $\psi(\cdot)$ denote an evaluation of the method outlined in Section 3.1 and $\rho^n = \rho(\cdot, t_n)$ where $t_n = n\Delta t$. Then we solve for the $n+1$ time step using the following scheme:

$$\begin{aligned} Y^{(1)} &= \rho^n + \Delta t \psi(\rho^n), \\ Y^{(2)} &= \frac{3}{4}\rho^n + \frac{1}{4}Y^{(1)} + \frac{\Delta t}{4}\psi(Y^{(1)}), \\ \rho^{n+1} &= \frac{1}{3}\rho^n + \frac{2}{3}Y^{(2)} + \frac{2\Delta t}{3}\psi(Y^{(2)}). \end{aligned}$$

To satisfy the CFL condition given in Equation 14 we manually selected Δt to be proportional to Δx for each example. For example, when working with Nonlinear Diffusion and a compactly supported attraction kernel, we needed to choose $10\Delta t = \Delta x$. This meant that the speed of this method across different grids was dependent on both the convergence rate of the PDE to its steady-state solutions and the spacing of the grid we used.

The implementation of the one and two dimensional schemes was done in Matlab, and our code is available at this github page. Furthermore, it is important to note that a computational bottleneck of this scheme is the convolution in formula 13. Fortunately, this can be sped up significantly using a Fast Fourier transform, from $O(n^2)$ FLOPS to $O(n \log n)$ FLOPS. We also vectorized our code wherever possible to take full advantage of Matlab.

4.2 One Dimensional Replication of Results

We start by replicating several of the one-dimensional results from Carillo *et al* [1]. All results are for large time behaviors of the solutions to Equation 1, restated here in 1D:

$$\begin{cases} \rho_t & = \frac{d}{dx}[\rho(H'(\rho) + V(x) + W * \rho)_x], \quad x \in \mathbb{R} \\ \rho(x,0) & = \rho_0(x) \end{cases}.$$

Attractive-Repulsive Kernel

We first consider the above equation with $W(x) = \frac{|x|^2}{2} - \ln(|x|), H(\rho) = 0$, and $V(x) = 0$, This has a unit-mass steady state given by

$$\rho_\infty(x) = \begin{cases} \frac{1}{\pi}\sqrt{2 - x^2}, & |x| < \sqrt{2} \\ 0, & \text{else.} \end{cases}$$

As Carillo *et al* did, we use an initial condition given by

$$\rho_0(x) = \frac{1}{\sqrt{2\pi}} e^{-x^2/2}.$$

In the left plot of Figure 1 we start from a scaled version of the stated initial condition ρ_0 such that

$$\int_{-2}^{2} \rho_0(x)dx = \int_{-2}^{2} \rho_\infty(x)dx.$$

This is a required step as both our numerical scheme and its the underlying equations are mass preserving. Furthermore, we require a finite numerical domain, in this case $[-2, 2] \subset \mathbb{R}$. Something else of note for this example is that because W is singular at zero, we cannot represent $\int_{C_i} W(x_i - s)dx/\Delta x$ as $W(x_i - x_i)$ as

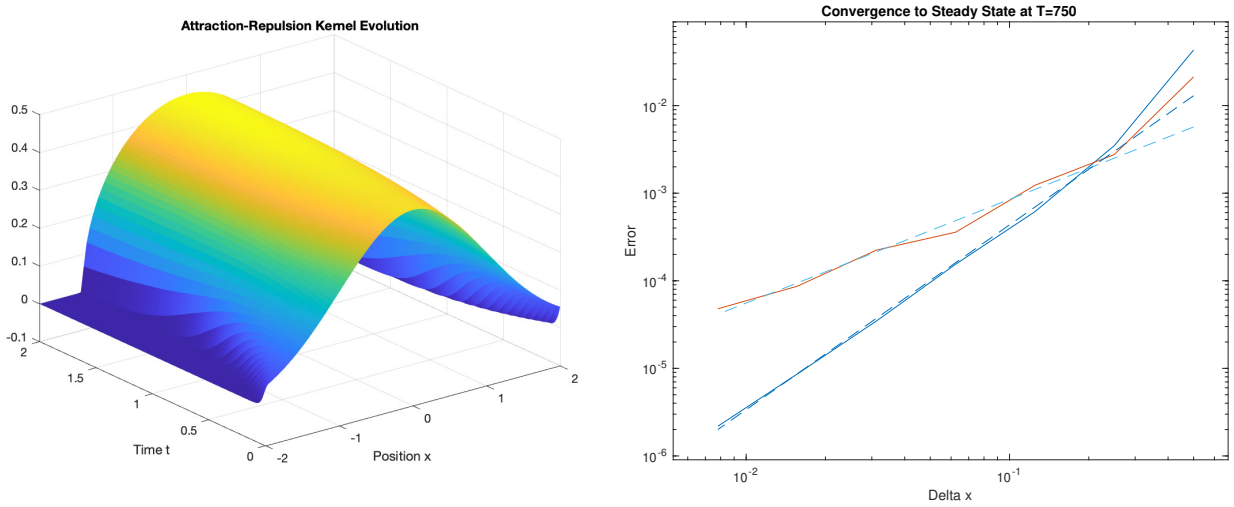

Figure 1: Left: Evolution of a Gaussian initial condition to the steady state of the singular attraction-repulsion kernel. Right: Convergence plot in L^1 (blue) and L^∞ norm (red). Dashed lines represent lines of slope 1.18 and 2.11, verifying the first and second order accuracy of the method in the L^∞ and L^1 norms.

we do implicitly in Equation 11. Instead, we must evaluate this integral of W explicitly and then plug the resulting value into each occurance of $W(x_i - x_i)$ in Equation 11. We see that

$$\frac{1}{\Delta x}\int_{C_i} W(x_i - s) = 1 + \frac{\Delta x^2}{24} - \ln\left(\frac{\Delta x}{2}\right).$$

Implementing this in Matlab for a variety of grid spacings Δx yields the right plot of Figure 1. This plot demonstrates the convergence of our error to zero in the L^∞ and L^1 norms. As in Carillo *et al*'s paper, we compute the L^1 norm using a piecewise constant approximation and evaluate the L^∞ norm using the cell centers only. This yields a second order convergence rate in the L^1 norm, as expected.

Nonlinear Diffusion with Nonlocal Attraction Kernel

We now consider Equation 1 while setting $W(x) = \frac{-\exp(-|x|^2/2\sigma)}{\sqrt{2\pi\sigma}}$, $H(\rho) = \frac{\nu}{m}\rho^m$, and $V(x) = 0$ with $\nu > 0$, $m > 1$, and $\sigma > 0$. In our experiments we have defined $m = 3$, $\nu = 1.48$ and $\sigma = 1$ and select an initial condition $\rho_0(x) = \frac{1}{\sqrt{8\pi}}\left(e^{-0.5(x-k)^2} + e^{-0.5(x+k)^2}\right)$ as Carillo *et al* did. The variable k denotes how far apart a pair of Gaussians are at the initial time 0. As seen below when k is larger it takes longer to converge towards the steady state solution of a single bump. However, this approach and final merger is inevitable as our attraction kernel is supported on all of $\mathbb{R}$.

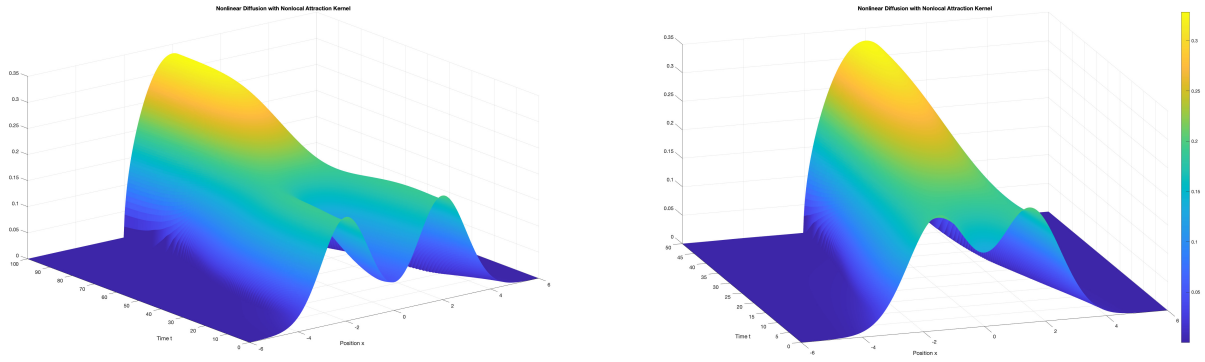

Figure 2: Evolution of a 1D Nonlinear diffusion equation with initial data given by a pair of Gaussians. Note how both appear to approach the same steady state, albeit at slightly different rates.

In Figure 2 note that the time axis on the left goes to $T = 100$, whereas the right only goes up to $T = 50$, further highlighting the difference in the speed of the convergence. Looking at the interaction potential, $W(x)$, this can be understood further as the function approaches 0 exponentially quickly with the magnitude of x. The further apart the Gaussians start, the less interaction force they have on each other through the convolution in Equation 11.

Nonlinear Diffusion with Compactly Supported Attraction Kernel

We now set $W(x) = -(1 - |x|)_+, H(\rho) = \frac{\nu}{m}\rho^m$, and $V(x) = 0$ in Equation 1. This has the same internal energy as from the previous experiment and again we have defined $m = 3$ and $\nu = 1.48$. We apply this PDE to an initial condition given by the uniform measure,

$$\chi_A(x) = \begin{cases} \frac{1}{\int_A 1dx} & x \in A \\ 0 & x \notin A \end{cases}.$$

The compactly supported kernel can give us markedly different behavior from the non-local kernel discussed previously. In the previous two examples they converged to a single connected component, while we show it is possible to find a steady state with three disconnected components. This behavior, demonstrated in Figure 3, is possible due to the compactly supported $W(x)$. The defined interaction potential is only supported on $(-1, 1) \subset \mathbb{R}$ and thus positions $x, y \in \mathbb{R}$ such that $|x - y| \geq 1$ do not impact each other's evolution through the convolution in Equation 11. The right-most plot of Figure 3 also demonstrates numerically that our scheme is in fact entropy-decreasing.

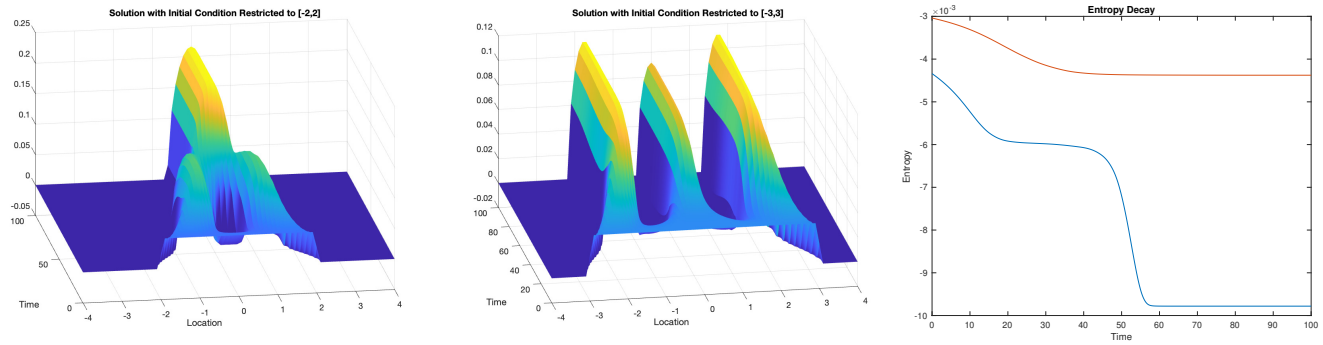

Figure 3: Decay of Entropy for Nonlinear Diffusion example with a Compactly supported attraction Kernel. Left: Evolution of solution with initial condition $\chi_{[-2,2]}(x)$. Two bump solutions initially form and seem stable for some time before drawing close enough together for the attraction kernel to merge them into a single bump with lower entropy. Center: Evolution of solution with initial condition $\chi_{[-3,3]}(x)$. Three bump solutions initially form, however they are far enough apart that the interaction kernel cannot merge them, resulting in them plateauing at an entropy much greater than the minimum possible entropy with this mass. Right: Plot demonstrating the decay of the numerical entropy. The blue curve corresponds to the solution shown on the right and the red curve corresponds to the solution shown in the center.

4.3 Two Dimensional Replication of Results

We now look at solutions to Equation 1 when $\mathbf{x} \in \mathbb{R}^2$.

Nonlinear Diffusion with Gaussian Kernel

We consider Equation 1 with $W(\mathbf{x}) = \frac{e^{(-|\mathbf{x}|^2)}}{\pi}, H(\rho) = \frac{\nu}{m}\rho^m$, and $V(\mathbf{x}) = 0$. The internal energy H is again taken from the 1 dimensional nonlinear diffusion experiments but we have selected $m = 3$ and $\nu = 0.1$, resulting in much less diffusion. The initial condition here is given by a scaled version of $\rho_0(\mathbf{x}) = \chi_{[-3,3]\times[-3,3]}(\mathbf{x})$ with non-unit mass, as done in Carillo *et al.* The time evolution can be seen in Figure 4. Although the initial state is a uniform distribution on $[-3, 3] \times [-3, 3]$, at $T = 1$ we see 4 peaks forming,

which become more distinct ($T = 5$) before merging into a single peak by $T = 10$. Similarly to before, the Gaussian kernel affects the evolution of the measure and causes the four nearly localized solution to form before they merge into a single bump.

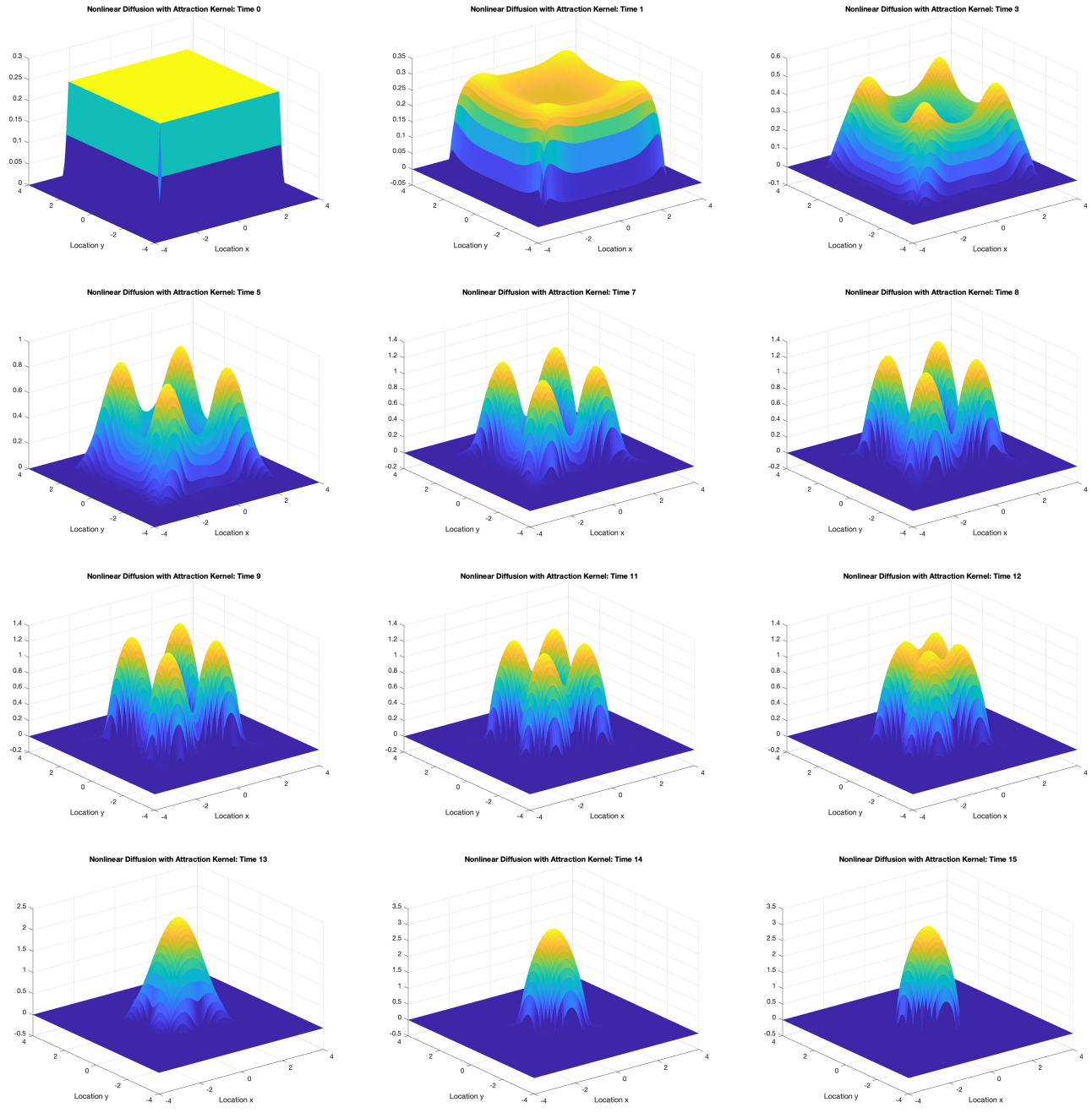

Figure 4: Evolution of a non-unit mass in two dimensions for the equation with nonlinear diffusion and a Gaussian kernel. From left to right and top to bottom, these represent times 0, 1, 3, 5, 7, 8, 9, 11, 12, 13, and 15. Note how, similar to the 1-D example, a number of individual bumps form before merging into a final steady state

5 Conclusion

Throughout this project we have replicated the work of Carillo *et al*, reporting on the motivations and form for their finite volume method in one dimension. We've also learned about this method's various properties

which make it suitable for problems of this form, and have applied it to a wide variety of examples in one and two dimensions. In the future, we would be interested in generalizing the method to a non-homogenous grid as Carillo *et al* have in one dimension, as well as investigating an extension of the non-homogenous grid to two dimensions. Furthermore, it would be interesting to compare our method to more examples, either those with different interaction potentials or internal energies, those where we have included a confining potential $V(x)$.

6 Acknowledgements

The authors thank Professors Hosseini and Hu for their input on the inclusion of convergence plots, as well as Wietse Vaes and Kaitlynn Lilly for helpful discussions while debugging the creation of those plots.

References

[1] José A Carrillo, Alina Chertock, and Yanghong Huang. A finite-volume method for nonlinear nonlocal equations with a gradient flow structure. *Communications in Computational Physics*, 17(1):233–258, 2015.

[2] Sigal Gottlieb, Chi-Wang Shu, and Eitan Tadmor. Strong stability-preserving high-order time discretization methods. *SIAM review*, 43(1):89–112, 2001.